*E-proceedings of the 38th IAHR World Congress*
*September 1-6, 2019, Panama City, Panama*
doi:10.3850/38WC092019-1546

# DAM-BREAK FLOW IN A CHANNEL WITH A 90° BEND AND MOBILE BED: EXPERIMENTAL AND NUMERICAL SIMULATIONS

SANDRA SOARES-FRAZÃO[1], STÉPHANIE ABBEELS[2], MARIE MESSENS[3]

[1,2,3] Institute of Mechanics, Materials and Civil Engineering (iMMC)
Université catholique de Louvain, Belgium
sandra.soares-frazao@uclouvain.be

## ABSTRACT

Predicting the morphological changes induced by fast transient flows such as flash floods or dam-break flows is still a challenging task, especially when sediment transport is considered. In order to validate numerical simulation tools designed for such flow conditions, reliable experimental data is needed. In this paper, dam-break flow experiments over a mobile bed made of coarse uniform sediments are presented. The initial conditions consist of a constant water-depth in the upstream reservoir and a saturated sediment bed downstream. Due to the strong reflection of the flow in the bend, complex morphological patterns can be observed, with significant erosion and deposition. Measurements were obtained using non-intrusive devices to capture the free-surface evolution as well as the bed morphological evolution. The free-surface evolution was measured using ultrasonic probes at several locations. The bed morphological evolution was measured using digital imaging devices and a laser-sheet to isolate given cross-sections of the flow on the images. Such a technique proved its efficiency in slower flow conditions, but its application to the present case with a fast flow involving significant sediment transport is challenging. These measurements are then compared to numerical simulations performed using a finite-volume scheme with a lateralized HLLC scheme for the flux predictions. This scheme solves in a coupled way the system composed by the shallow-water equations and the Exner equation for the bed morphology, closed by the Meyer-Peter and Müller formula for sediment transport. Finally, a discussion of the numerical results is proposed, through the comparisons with the experimental data.

**Keywords:** sediment transport, dam-break, erosion, deposition, 90° bend

## 1 INTRODUCTION

Nowadays many dams built in the previous century are becoming old and worn out. Combined with the global climate change inducing new extreme conditions, dam failures are more and more likely to occur. Unfortunately, a dam break is quite complicated to predict and therefore it is hard to estimate the risk of flooding for the population that lives underneath. The need for accurate numerical simulations is of paramount importance in order to be able to assess this risk. However, as field data measured during real events are scarce, reliable experimental measurements are needed to validate numerical simulation tools designed for such flow conditions.

When such a flow occurs over a movable bed, the associated erosion and the deposition processes can be very substantial and can reshape the valley downstream showing the importance of taking those morphological changes into consideration for risk assessment and rescue planning. In the present study, a dam-break flow in a channel with a sharp bend is considered, where it appears that sediment transport in the bend induces complex morphological patterns and significantly modifies the flow.

Up to now, no numerical model allows to predict accurately the phenomenon of sediments transport in a two-dimensional (2D) configuration under the propagation of a rapid water wave in an erodible channel. A huge variability also exists between the models used to predict those morphological changes as illustrated by a benchmark test for numerical models between 12 worldwide teams of researchers over a same problem situation of dam break flow (Soares-Frazão et al., 2012). The main difficulties are the fast-transient flow combined to an intense transport of sediments and a 2D geometry.

Regarding numerical simulations, this paper illustrates the strengths and limits of a numerical model that has already been proved efficient for fast transient flows, especially dam-break flows over a horizontal fixed bed (Soares-Frazão and Zech, 2010) complemented with a bank failure operator developed by Swartenbroekx et al. (2010). The numerical model is based on the Saint-Venant-Exner equations and its resolution is based on a fully coupled finite-volume model and an adapted HLLC (Harten-Lax-Van Leer with contact discontinuities) solver for the flux considering a new wave-speed estimator (Soares-Frazão and Zech, 2010).

In order to assess the efficiency of the numerical model, an experimental setup of a channel with a 90° bend and an erodible bed made of uniform coarse sand is used to further investigate sediment transport and morphological evolution is severe transient flow conditions. The main objective of this work is twofold: (1) provide a new reliable data set for the validation of numerical models and (2) investigate the capabilities and limits of a finite-volume scheme based on the Saint-Venant-Exner equations to reproduce strong morphological evolution.

In this paper, the physics of the flow is first described, then the measurement techniques used to obtain water-level and bed evolution measurements are presented. The numerical model is briefly described and finally the experimental and numerical results are compared.

## 2 FLOW DESCRIPTION

In reality, there are various types of bends in a river: smooth and long curves or sharp and narrow bends. In smooth curves with steady flows, the sediments tend to deposit on the inner side of the curve, while the outer side is eroded. The curve creates a change in the free-surface inclination, which makes the water level rise on the outer side whereas its inner side is lower. However, in a fast-transient flow, the behaviour is not the same, even more in the case of sharp and narrow bends. Such a flow is reproduced here through the idealized example of a channel with a sharp 90-degree bend.

The flow is illustrated in Figure 1. The dam-break induces a supercritical flow that undergoes a sudden change in direction when reflected against the bend. When it reaches the bend, a water column rises, and the velocity of the flow becomes almost zero (Figure 1a). Then, the water column collapses and a new water front appears both upstream and downstream (Figure 1b). A hydraulic jump is formed and goes back upstream until it reaches the reservoir (Figure 1c, Figure 1d). This jump produces a subcritical flow that moves slower than the supercritical flow that exits the dam. After this transient phase, the flow reaches an almost steady state and the free surface inclination in the bend reacts in the same way as the one described previously, that can be observed in steady flows.

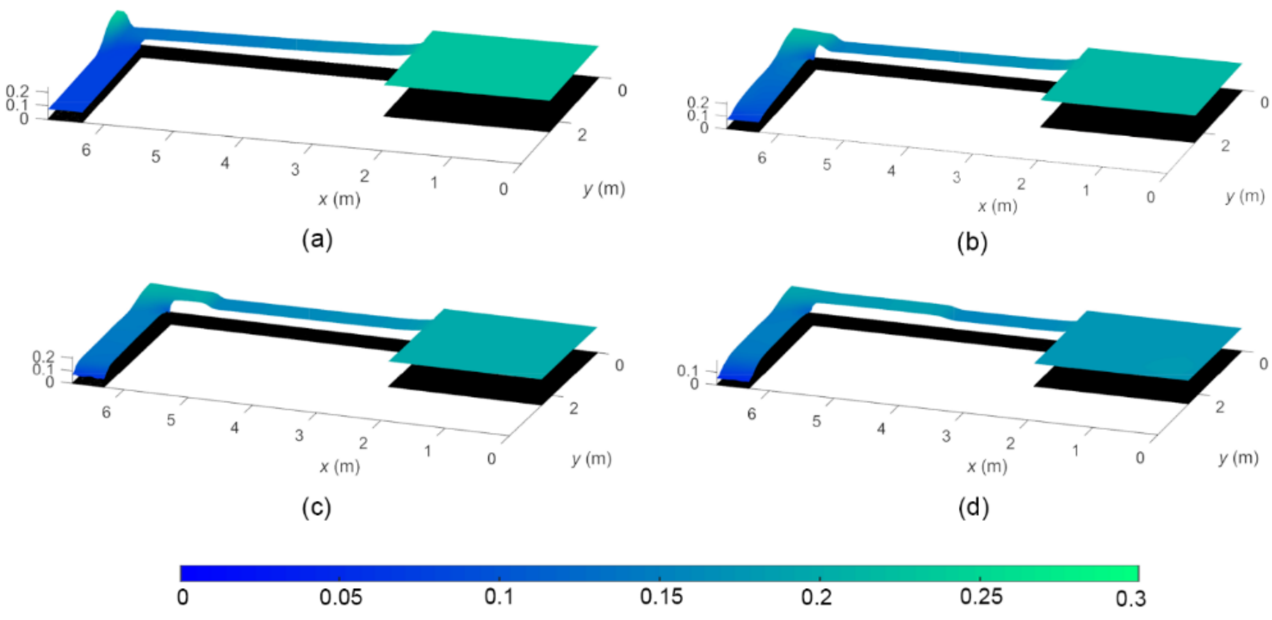


**Figure 1.** Water level (m) of the dam-break flow for (a) 3s, (b) 5s, (c) 7s and (d) 11s.

The sudden change can also be explained in terms of energy. The kinetic energy prevailing in the supercritical phase, is transformed into potential energy when the water is stopped at the bend and rises. While the kinetic energy is described in terms of velocity vectors having a certain direction, the potential energy has no direction and is only a scalar value. When the water column collapses, the potential energy is transformed again into kinetic energy, but the direction has changed.

Sediment transport in a sharp bend with a fast-transient flow is more complicated to describe than in steady flow conditions. The sediments will follow the water wave and deposition will be found on the outer side of the bend because the flow detaches from the wall as it cannot follow the sharp angle. Some deposition will also be found in the inner side of the bend, because of different factors such as the water and sediment recirculation.

These complex patterns will have to be carefully monitored using non-intrusive techniques as described in the next section.

## 3 EXPERIMENTAL SETUP AND MEASUREMENT TECHNIQUES

The experimental setup used to describe the behaviour of the sediments is located in the Civil Engineering Department of the Université Catholique de Louvain, Belgium, and is illustrated in Figure 2. The reservoir has dimensions of 2.44 m x 2.39 m. Attached to it is a rectangular channel with glass walls, 0.495 m wide and with a reach of approximately 4 m upstream of the bend and 3 m downstream. The reservoir bed level is 0.33 m below the channel bottom and on this latter, 0.075 m of coarse uniform sediments are packed. The downstream end of the channel is a free fall. The initial water level in the reservoir reaches 0.26 m above the channel bed, hence 0.185 m above the mobile bed level, and the sediment are initially almost saturated. The Manning roughness coefficient of the sand bed was measured under steady flow conditions and the value used is 0.0165 (Soares Frazão et al., 2012). The dam-break is simulated with the sudden rise of the gate between the reservoir and the channel. The experiment is run for 60 s, then the gate is closed, and the channel slowly empties. As no more visible sediment transport occurs after 60 s, the resulting bed morphology when the channel is empty of water is considered as the final situation.

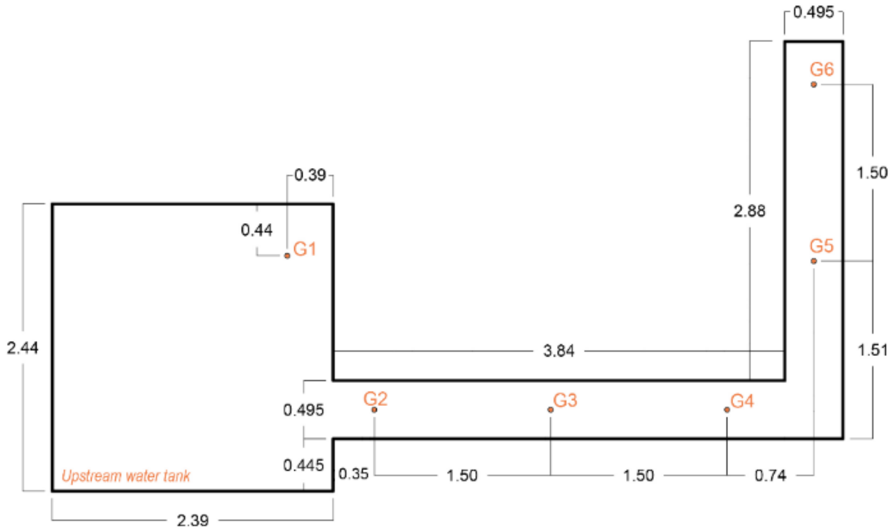


**Figure 2.** Plan view of the channel with a 90° bend. Dimensions in (m).

Several non-intrusive techniques were used in order to asses various characteristics of the flow. The temporal evolution of the water level was measured by means of six ultrasonic gauges placed above the channel and the reservoir as illustrated in Figure 2.

The bed morphological evolution was evaluated with a high-speed camera located next to the channel. Pictures are taken at a rate of 62 frames per second, for a given section of the flow enlighten by a laser sheet projected on the sediment bed. Thanks to the laser-sheet illumination, the limits of the water and bed surfaces can be identified on the images.

In Figure 3a, both lines are well captured, and it is possible to distinguish which laser reflection is on the sand and on the water. In Figure 3b however, the water level $z_w$ is too low and is blocking the view of the laser beam reflection on the sediments. If the level decreases even more, the sediment line will not be visible at all. When there is only one line visible, no assumption can be made to know if that line represents the free surface of the water or the sediment bed, so the line shown cannot be taken into account to represent the evolution of the bed. Resolving this issue was an important part of the experimental modelling, in order to obtain correct values to compare with the numerical model.

So, the difficulty with this technique is to correctly position the camera to capture both lines. This is a complicated issue because of the reflection of the laser sheet on the free surface of the water. Therefore, the camera has to be positioned high enough with respect to the water level to capture it but low enough to see the laser beam on the sediment bed. This idea can be seen in Figure 4, where in (a) the water level is too low and so only the line of the free surface can be captured in (c) the water level is too high with respect to the camera so only the reflection line on the mobile bed is seen and finally in (b) the camera is correctly positioned and both lines are visible.

 

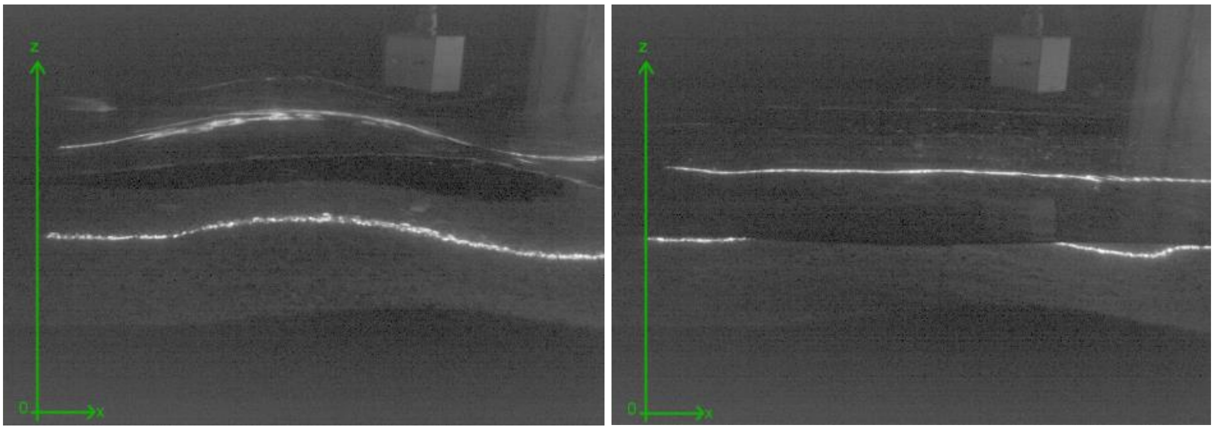

(a) (b)

**Figure 3.** Example of the reflection of the laser, (a) both lines are visible and (b) the sand is partially occulted.

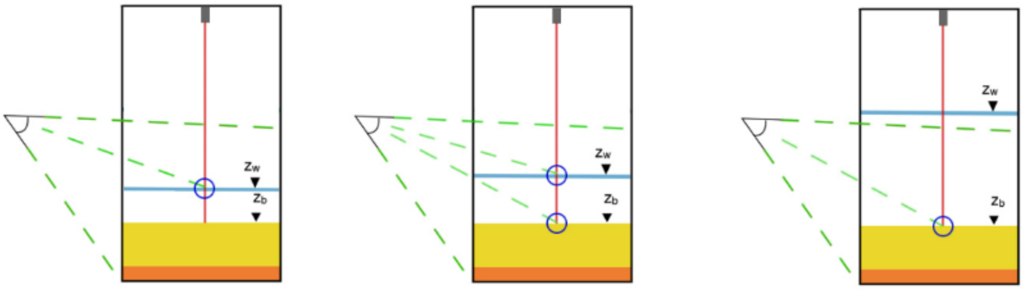

(a) (b) (c)

**Figure 4.** Lines captured by the camera with respect to the level of the water $z_w$.

The laser sheet and high-speed camera have also been used to measure the final topography of the channel, 60 seconds after the dam-break. A grid of 5 cm x 5 cm was used to obtain a detailed bed elevation model in the bend area.

## 4 NUMERICAL MODEL

### 4.1. Governing equations

The numerical model used in this study is an extension of the validated 1D Clear Water Layer model (CWL) over a movable bed (Van Emelen, 2014) to a 2D model. This model is based on the 2D model proposed by Soares-Frazão and Zech (2010) solving the Saint-Venant—Exner (SVE) system of equations

$$\frac{\partial \mathrm{U}}{\partial \mathrm{t}}+\frac{\partial \mathrm{F(U)}}{\partial \mathrm{x}}+\frac{\partial \mathrm{G(U)}}{\partial \mathrm{y}}=\mathrm{S} \qquad [1]$$

$$\boldsymbol{U}=\begin{pmatrix} h \\ uh \\ vh \\ zb \end{pmatrix}=\begin{pmatrix} h \\ q_x \\ q_y \\ zb \end{pmatrix};\ \boldsymbol{F}=\begin{pmatrix} q_x \\ \frac{q_x^2}{h}+\frac{gh^2}{2} \\ \frac{q_x q_y}{h} \\ \frac{q_{s,x}}{1-\varepsilon_0} \end{pmatrix}=\begin{pmatrix} q_x \\ \sigma_x \\ \mu_{xy} \\ \frac{q_{s,x}}{1-\varepsilon_0} \end{pmatrix};\ \boldsymbol{G}=\begin{pmatrix} q_y \\ \frac{q_x q_y}{h} \\ \frac{q_y^2}{h}+\frac{gh^2}{2} \\ \frac{q_{s,y}}{1-\varepsilon_0} \end{pmatrix}=\begin{pmatrix} q_y \\ \mu_{xy} \\ \sigma_y \\ \frac{q_{s,y}}{1-\varepsilon_0} \end{pmatrix};\ \boldsymbol{S}=\begin{pmatrix} 0 \\ gh(S_{0,x}-S_{f,x}) \\ gh(S_{0,y}-S_{f,y}) \\ 0 \end{pmatrix} \qquad [2]$$

in which $x$ and $y$ are the coordinates in a Cartesian system, $h$ represents the water-depth, $z_b$ the erodible bed level, $q_x = hu$ and $q_y = hv$ are the unit discharges in $x$- and $y$- directions, with $u$ and $v$ the depth-averaged velocity components, $q_{s,x}$ and $q_{s,y}$ the unit solid flow rates in the $x$ and $y$ directions, and $\varepsilon_0$ the porosity of the bed. The components $S_{0,x}$ , $S_{0,y}$ and $S_{f,x}$ , $S_{f,y}$ of the source term vector $S$ correspond respectively to the bed slopes and the friction slopes in the $x$ and $y$ directions.

The sediment transport rate $q_s$ is found by solving a closure equation. In this study, the Meyer-Peter and Müller (MPM) sediment transport formula is used. It is defined as:

$$q_s(q,h)=8\sqrt{g(s-1)d_{50}^3}(\max(0,\tau_*-\tau_{*C}))^{3/2} \qquad [3]$$

where $s$ denotes the ratio between the sediment and water density and $d_{50}$ is the representative grain diameter. The non-dimensional bed shear stress $\tau_*$ can be expressed as

$$\tau_* = \frac{n^2 q^2}{(s-1) d_{50} h^{7/3}} \ , \qquad [4]$$

where $q = \sqrt{q_x^2 + q_y^2}$ is the water unit discharge and $n$ is the Manning friction coefficient.

The sediment motion is considered to start when $\tau_*$ exceeds a certain threshold corresponding to the non-dimensional critical bed shear stress $\tau_{*c}$ ($\tau_{*c} = 0{,}047$ for MPM). This closure equation can be extended to a two-dimensional case by considering the x and y components of the shear stress calculated with the x- and y-components of the unit-discharge.

This system of equations is solved numerically by using a first-order finite volume scheme over an unstructured triangular mesh, written as

$$\mathrm{U}_i^{\mathrm{n+1}} = \mathrm{U}_i^{\mathrm{n}} - \frac{\Delta t}{\Omega_i} \sum_{j=1}^{n_b} \mathrm{T}_{\mathrm{j}}^{-1} \mathrm{F}_j^* (\overline{\mathrm{U}}_j) L_j + \mathrm{S}_{\mathrm{F,i}} \Delta t \qquad [5]$$

Where (Figure 5) $\Omega_{\mathrm{i}}$ is the cell-base area, $L_j$ the j-interface length and $n_b$ the number of cell interfaces (3 for a triangular cells). The inter-cell fluxes are calculated using a HLLC scheme (Toro et al. 1997), the friction slope term is calculated using Manning's formula while the $S_0$ components are treated in efficient lateralised way (Fraccarollo et al. and Costanzo et al.).

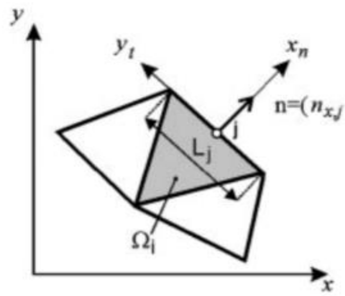


**Figure 5.** Unstructured mesh finite-volume discretisation (S. Soares-Frazão and Y. Zech, 2010)

4.2. Bank failure

In order to account for lateral erosion and therefore mass failure of local unstable steep sediment slopes, a two-dimensional bank failure operator was developed and inserted into the classical 2D shallow-water model (SVE) by Swartenbroekx et al. (2010). The operator updates the deposition and erosion of the bottom by comparing locally the slope of the bed to the stability angles of the sediments considering material homogeneity and saturation. It allows to simulate as close to the reality as possible the behaviour of the sediments in the channel.

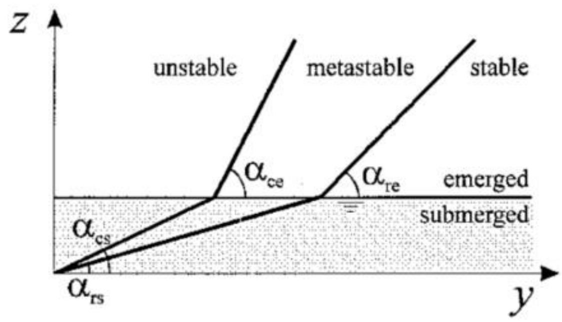


**Figure 6.** Definition of stability angles (Swartenbroekx et al., 2010)

The criterion suggests that when the slope of a cell of the mesh exceeds a critical angle $\alpha_c$, the bank failure is activated, and cells are tilted until reaching a residual angle $\alpha_r$ (Zech et al, 2008) (See Figure 6).
The values of the angles to be used for a certain material can be determined experimentally (Spinewine et al.,2002). The critical and residual angles for the sand, respectively emerged and submerged, used in this study are $\alpha_{ce} = 87°$; $\alpha_{cs} = 35°$; $\alpha_{re} = 85°$; $\alpha_{rs} = 30°$.

 

4.3. Geometry and boundary conditions

The computational domain is discretised in 4137 triangular elements as illustrated in Figure 7. Wall boundary conditions are used all along the domain except at the downstream end of the channel where a free outflow is considered by means of a transmissive boundary condition. According to Savary and Zech (2007), in the case of a transmissive boundary condition for the hydrodynamic part of the flow, a downstream sediment level has to be imposed. This level is imposed here as the fixed bed level of the channel in order to reproduce the experiment in the best possible way.

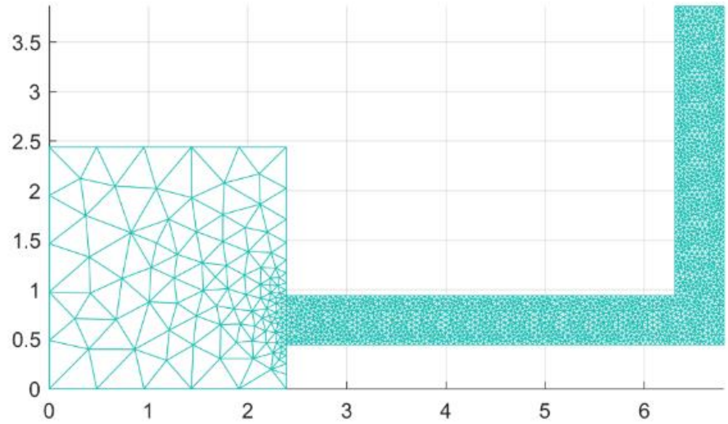


**Figure 7.** Mesh used in the numerical model

## 5 COMPARISON BETWEEN EXPERIMENTAL AND NUMERICAL MODEL

By means of the digital imaging technique that was previously described, three types of comparisons were made between the numerical and the experimental models: the water level at the gauging points, the final bed topography and the evolution of the bed elevation in two different zones.

5.1. Water level

With the ultrasonic gauges located as on Figure 2, the water level was measured during the dam-break flow. In an equivalent way, it was obtained numerically. The results shown in Figure 8 prove that the experimental and numerical modelling are in very good agreement.

Figure 8 shows the evolution of the water level in the upstream channel section, for the experimental and the numerical models. To start, it is clear that the reservoir empties at the same rate in both cases (Figure 8a, Gauge 1), indicating that the correct discharge is computed from the reservoir. Then, looking front wave arrival time, there is a good match for each gauge (Figures 8b-d). The wave reaches Gauge 2 (Figure 8b) after less than a second since it is the closest to the door, then Gauge 4 (Figure 8d) after approximately 2 seconds. The speed of the wave is thus well evaluated by the numerical model. The water level is also well reproduced, except for the initial peak at Gauge 2 that is a little bit underestimated, even though this difference is not so relevant.

The hydraulic jump issued from the wave reflection in the bend happens at Gauge 2, Gauge 3 and Gauge 4 a second earlier than in reality. This means that the velocity of the jump is overestimated in the numerical model. It reaches Gauge 4 after 6,7 seconds numerically and after 7,6 seconds experimentally. The same happens at Gauge 2 where the jump arrives after 14 seconds numerically and after 15,2 seconds experimentally. The mean height of the jump is well reproduced for all gauges, but the model is not able to reproduce the surface waves that are observed in the experimental measurements. As it will be detailed further, these surface waves are related to the appearance of antidunes in the upstream reach.

 

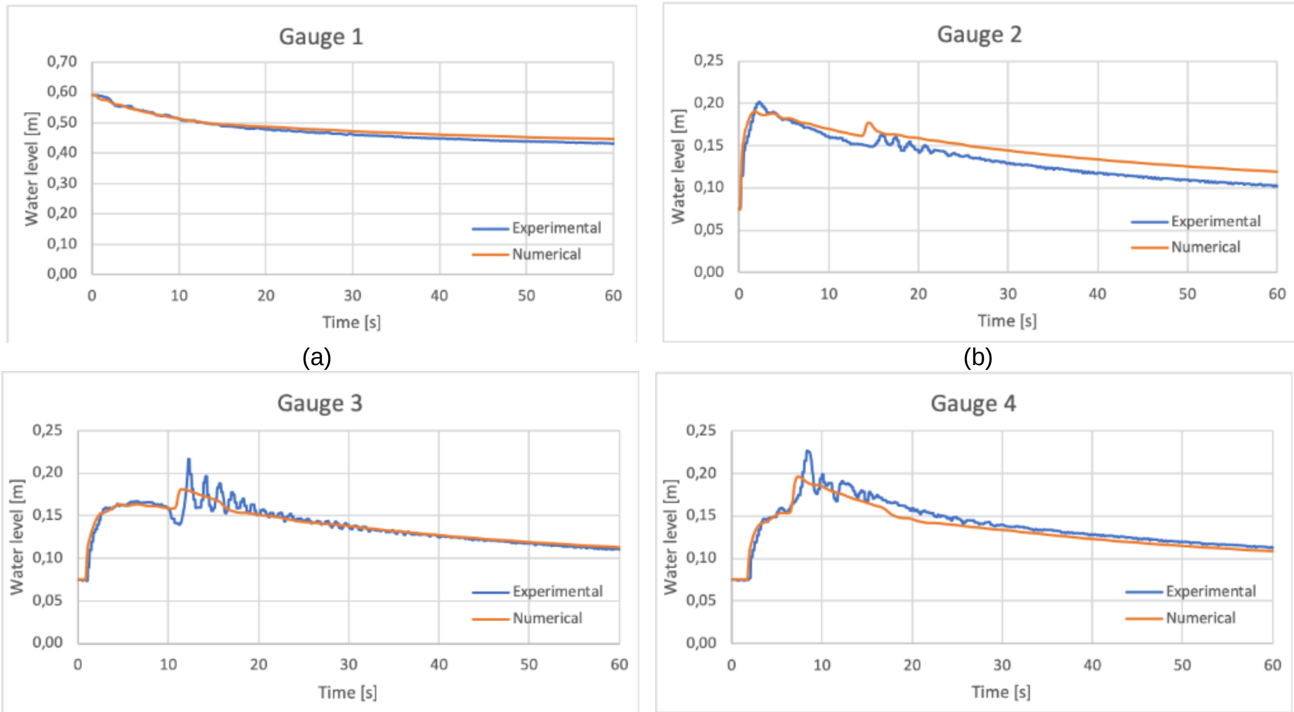


(a) (b)

(c) (d)

**Figure 8**. Water level for (a) gauge 1, (b) gauge 2, (c) gauge 3, (d) gauge 4.

Figure 9 shows the comparison of the evolution of the water level in the downstream part of the channel (Gauge 5 and Gauge 6). The numerical model overestimates a little bit the velocity of the subcritical wave, hence the water reaches the gauges almost 1 second too early. Apart from that, the water level and the emptying rate are quite similar for the fifth gauge. In the last case, the water level is quite overestimated between seconds 5 to 12 for Gauge 6 (Figure 9b). This might be explained by an underestimation of the bed erosion in this area, as will be detailed in the next sections, or by the transmissive boundary conditions imposed at the exit of the channel. Overall, the shape given by the numerical model follows quite well the one of the experimental and both models can be considered in good agreement, at least in terms of water level.

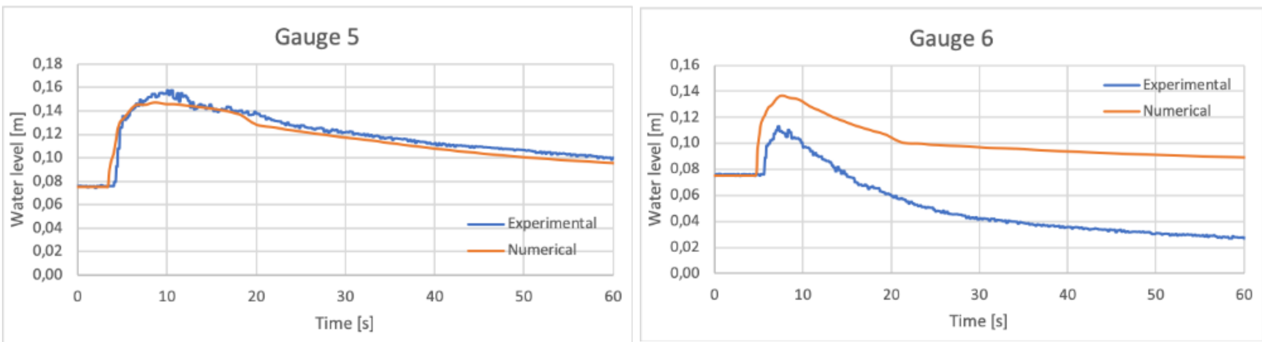


(a) (b)

**Figure 9.** Water level for (a) gauge 5, (b) gauge 6.

5.2. Final topography of the sediment bed

In order to properly compare the bed morphological evolution, it is important to start with the final topography of the channel. Figure 10a shows the topography obtained experimentally with the laser sheet technique, 60 seconds after the opening of the door. Figure 10b shows the same bed topography but obtained numerically. This comparison clearly demonstrates the limits of the numerical model that significantly underestimates the erosion and deposition processes, especially in the bend area. This will be developed in a further section.

Figure 10c showing the same computed results as Figure 10b with a different scale, shows that although the process is underestimated, the global shape of erosion and deposition processes is reproduced, with deposition at the inner side of the bend.

 

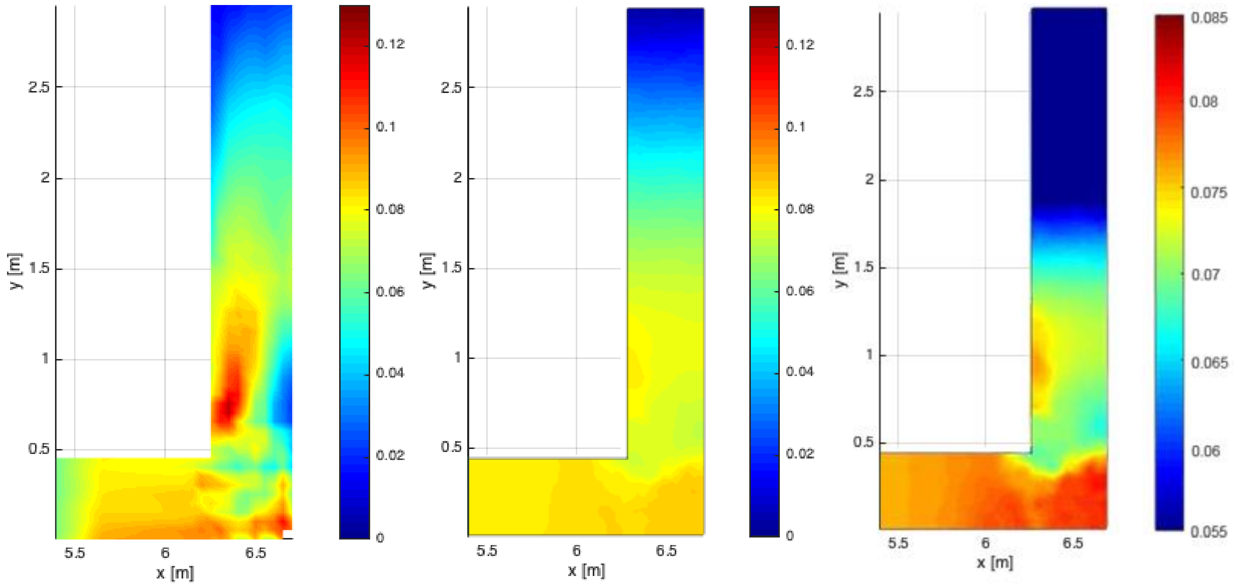

(a) (b) (c)

**Figure 10.** Bed topography after 60s, (a) experimentally, (b) & (c) numerically obtained.

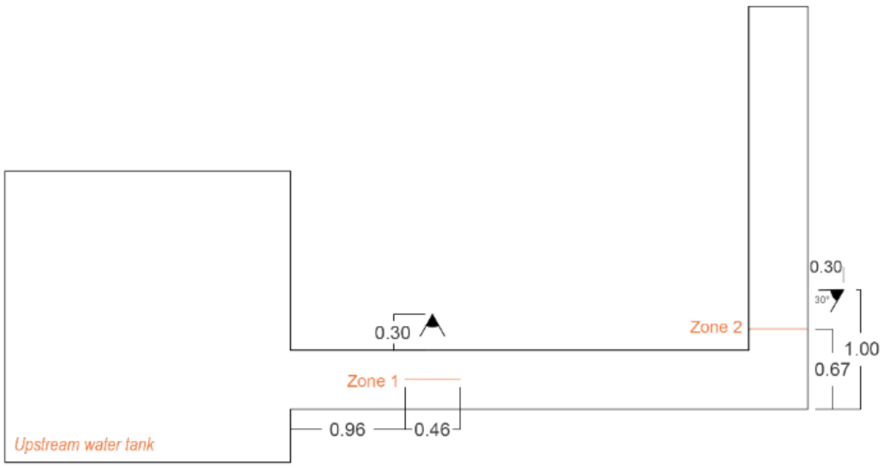


**Figure 11.** Plan view of the placement of the laser sheets and cameras.

## 5.3. Evolution of the bed level

With the laser sheet technique providing bed evolution measurements during the experiment, two different zones are analysed, as shown in Figure 11 : one in the first section of the channel (zone 1) and the other right after the bend (zone 2). In the first zone, the laser sheet is placed lengthwise at 0.96 m from the door of the reservoir and has a length of 0.96 m. The camera is positioned perpendicularly to the flow. In the second zone, the laser sheet is perpendicular to the flow, it has the width of the channel and it is placed 0.67 m from the outer point of the bend. The camera is inclined with an angle of 30° and placed 1.00 m from the bend.

### 5.3.1. Evolution of the antidunes

The experiment in the first zone shows the formation and evolution of antidunes (Figures 12-13). An antidune is a bedform found in rivers or channels during supercritical flows. It presents itself as a form of ripple on the sediment bed similar to a sand dune. When the door opens to simulate a dam-break, the flow is supercritical and antidunes start to form in the upstream section of the channel. In Figure 12, where the water flows from left to right, the final topography of the bed is illustrated in the zone where those antidunes form. Figure 13 shows their evolution at different times. It is noted that the evolution of the antidunes stops after approximately 10 seconds. It makes sense since the hydraulic jump that has formed on the bend had enough time to move back up (as can be seen in Figures 8a and b, for the gauges between which the profile is measured) and the flow has become subcritical.

Unfortunately, the numerical model does not take this phenomenon into account since the depth-averaged equations are not able to reproduce such features. The comparison with the numerical model is thus useless and not shown here.

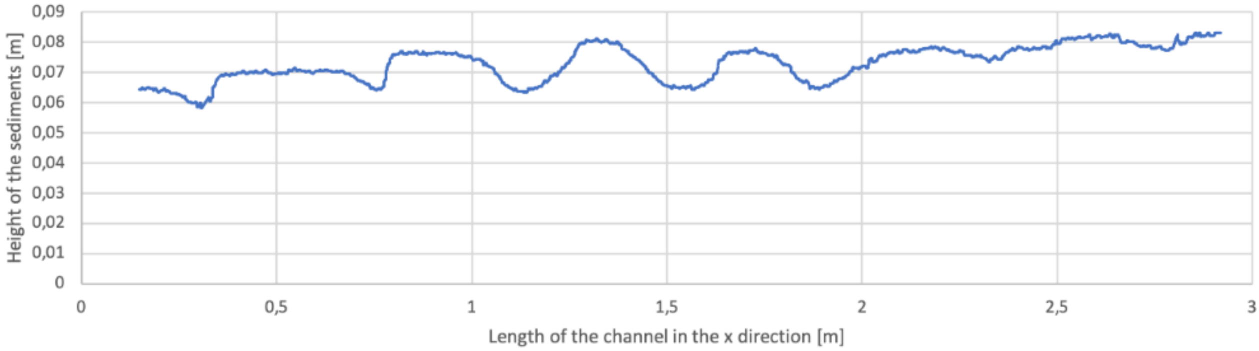


**Figure 12.** Longitudinal profile of the antidunes after 60 seconds.

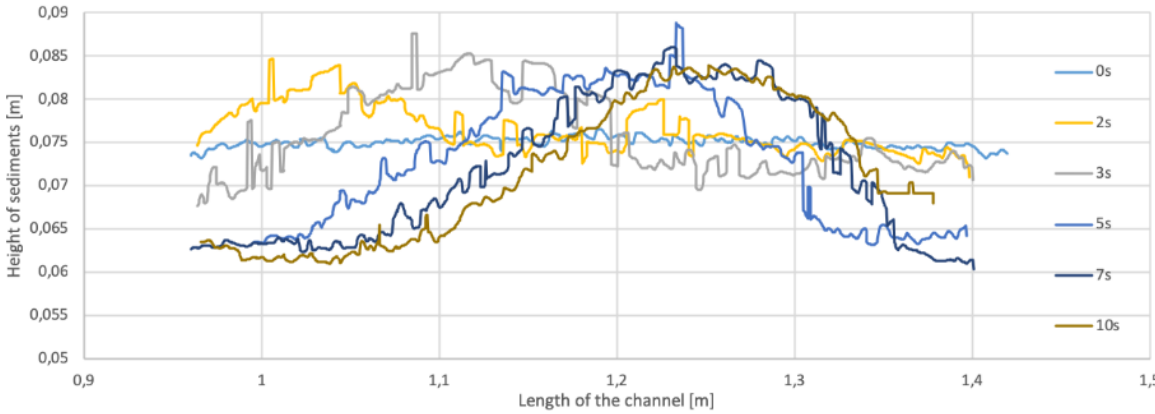


**Figure 13.** Evolution of the bed in the first zone for the first 10 seconds and (b) for the first 60 seconds.

5.3.2. Erosion and deposition in the bend

As seen in the map of the final topography in Figure 10, the erosion and the deposition in the bend are not well represented by the numerical model. The experimental evolution of those phenomena can be observed in the left part of Figure 14 (a, c and e). The inner part of the bend is located on the left side of the figure, where the deposition is pronounced: it reaches 12 cm in height. The erosion goes lower than 2 cm. By comparison, Figure 14b, 14d and 14f show the evolution of the bed level, obtained from the numerical simulations at the same time instants, but with a different scale. Indeed, the maximum bed level does not go higher than 7.47 cm and the minimum lower than 6.71 cm, so the curve would appear as almost horizontal if the same scale as the experiements was used. With the adapted scale, even though it is clear that both the erosion and the deposition are severely underestimated, it is possible to highlight that the curve still seems to have a shape comparable to the experimental one. Indeed, erosion is found on the outer side of the bend whereas deposition is shown on the inner side. So, the numerical model underestimates several characteristics of the flow, but the general idea is still conserved.

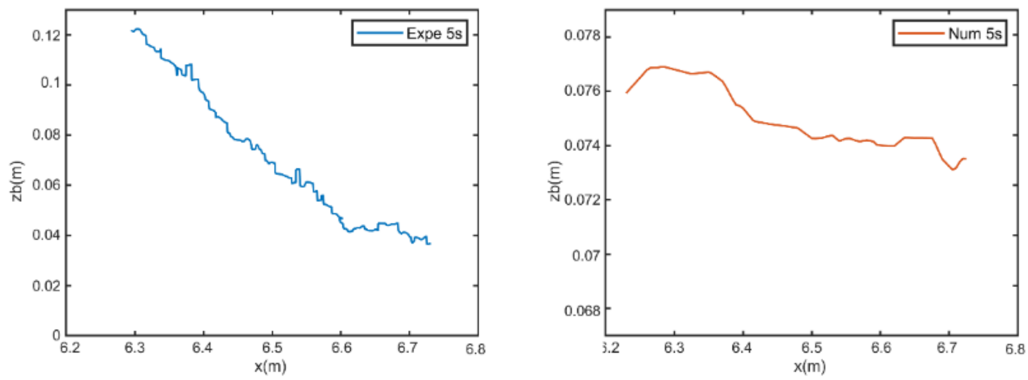


 

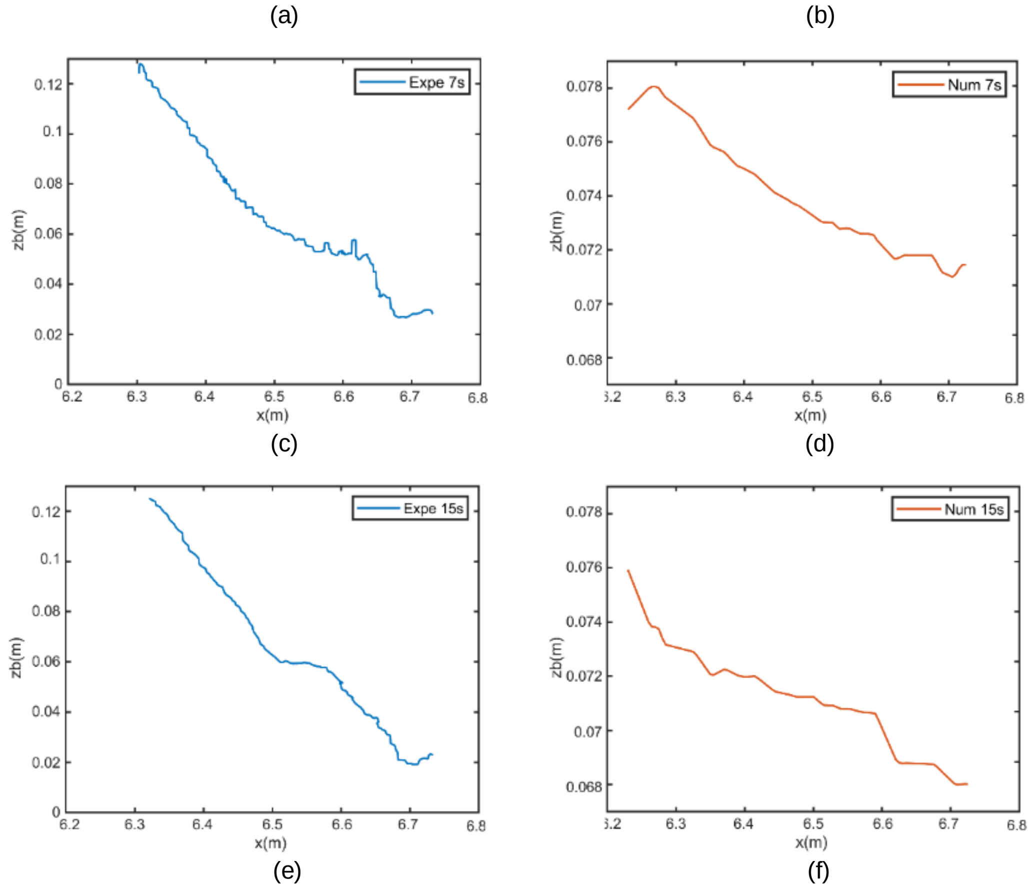


**Figure 14.** Evolution of the bed in the second zone, experimentally in blue and numerically in orange.

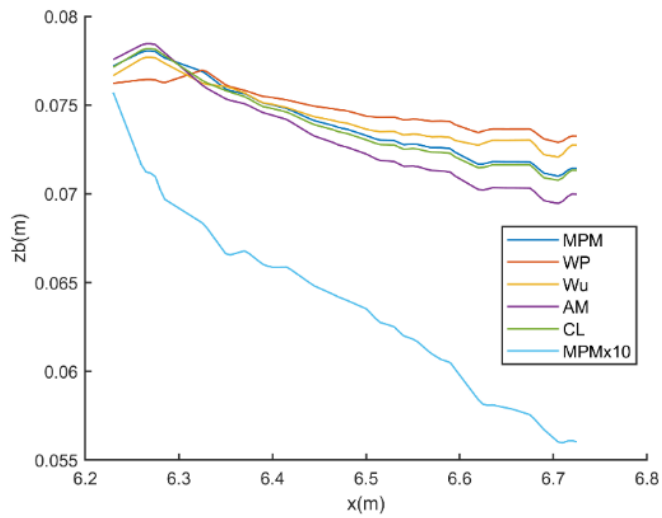


**Figure 15.** Final bed topography in the bend: influence of the transport equation used

Considering the underestimation of erosion and deposition processes by the numerical model, the choice of the sediment transport equation used for the calculations is questioned. In order to verify its impact, several transport equations were implemented in the numerical model: Meyer-Peter and Müller, Wong & Parker, Wu et al., Camenen & Larson (Van Emelen, 2014) and Ashida & Michiue (Soares-Frazão et al., 2010). The comparison between those can be seen in Figure 15 for the final situation (i.e. after 60 s), with the light blue curve representing calculations made with Meyer-Peter and Müller formula multiplied arbitrarily by a factor of 10. It depicts that, even though some differences can be observed, none of the models describes accurately enough the erosion and deposition phenomena. Therefore, the difference cannot be attributed solely to the equation used. Other mechanisms are probably not considered in the numerical model, such as, for instance, the horizontal and vertical recirculation of the water and sediments in the bend, and that causes the important difference in bed level evolution observed.

## 6 CONCLUSION

This paper presents new experiments of dam-break flow over a mobile bed in a complex geometry, and numerical simulations using the two-dimensional shallow-water-Exner equations. From the comparisons between experimental and numerical results, it appears that several factors and processes need to be taken into account when modelling fast transient flows over mobile beds. However, not all these processes are included in the model equations, hence the differences found between numerical and experimental results. In this paper, the focus was put on reducing the error gap between those models but also on providing a set of experimental data usable for good comparisons.

First of all, the comparison of the water level in the channel allowed to validate partially the numerical model. However, the analogy in terms of sediment bed level is not as satisfying since the numerical model underestimates significantly the observed bed level. Erosion and deposition phenomena are noticed in the bend but with an amplitude far lower than in reality. This is caused by all the phenomena not considered in the numerical model, such as the recirculation of the water and sediments in the bend.

Dam-break flows are thus complicated to model since they imply intense velocities and quick changes of the morphology of the valley. This paper tries to offer an overview of this problem and of the current limitations of classical numerical modelling approaches. Future work will be devoted to the improvement of the recirculation process model in the bend.

## 7 REFERENCES

Costanzo, C., Macchione, F. & Viggiani, G. (2002). *The influence of source terms treatment in computing two dimensional flood propagation*. Proceedings of River Flow 2002, Louvain-la-Neuve, Belgium, vol. 1, 2002; 277–282.

Fraccarollo, L., Capart, H. & Zech, Y. (2003). *A Godunov method for the computation of erosional shallow water transients*. International Journal for Numerical Methods in Fluids 2003 41(9):951–976.

Le Grelle, N., Soares Frazão, S., Spinewine, B. & Zech, Y. (2007). *Dam-break induced morphological changes in a channel with uniform sediments: measurements by a laser-sheet imaging technique*. Journal of Hydraulic Research, 45, 87-95.

Savary, C. & Zech, Y. (2007). Boundary conditions in a two-layer geomorphological model. *Application to a hydraulic jump over a mobile bed.* Journal of Hydraulic Research - Vol. 45, no. 3, p. 316-332 (2007)

Soares Frazão, S. & Zech, Y. (2002). *Dam break in channel with 90° bend.* Journal of Hydraulic Research, 128:11, 956-968.

Soares-Frazão, S., Canelas, R., Cao, Z., Cea,L., Chaudhry, HM., Die Moran, A., El Kadi, K., Ferreira, R. Fraga Cadórniga, I., Gonzalez-Ramirez, N., Greco, M., Huang, W., Imran, J., Le Coz, J., Marsooli, R., Paquier, A., Pender, G., Pontillo, M., Puertas, J., Spinewine, B., Swartenbroekx, C., Tsubaki, R., Villaret, C., Wu, W., Yue, Z. & Zech, Y. (2012). *Dam-break flows over mobile beds: experiments and benchmark tests for numerical models*. Journal of Hydraulic Research, 50:4, 364-375.

Soares-Frazão, S. & Zech, Y. (2010). *HLLC scheme with novel wave-speed estimators appropriate for two-dimensional shallow-water flow on erodible bed*. Int. J. Numer. Meth. Fluids 2011; 66:1019–1036

Spinewine, B., Zech, Y. (2002). *"Geomorphic Dam-Break Floods: Near-Field and Far-Field Perspectives"*. IMPACT Investigation of Extreme Flood Processes and Uncertainty (CD-ROM).

Swartenbroekx, C., Soares-Frazão, S., Staquet, R. & Zech, Y. (2010). *Two dimensional operator for bank failures induced by water-level rise in dam-break flows.* Journal of Hydraulic Research, 48(3), 302-314

Toro, EF. (1997) *Riemann Solvers and Numerical Methods for Fluid Dynamics. A Practical Introduction.* Springer: Berlin, Germany, 1997.

Van Emelen, S. (2014). *Breaching processes of river dikes: effects on sediment transport and bed morphology.* PhD thesis, Université catholique de Louvain, Belgium

Zech, Y., Soares Frazão, S., Spinewine, B. & Le Grelle, N. (2008). *Dam-break induced sediment movement: Experimental approaches and numerical modelling*. Journal of Hydraulic Research Vol. 46, No. 2 (2008), pp. 176–190.

 